



1 Mediterranean Outflow Water variability during the Early 2 Pleistocene climate transition

3 Stefanie Kaboth¹, Patrick Grunert², Lucas J. Lourens¹

4 ¹ Department of Earth Sciences, Faculty of Geosciences, Utrecht University, Heidelberglaan 2, 3584 CS, Utrecht, The
5 Netherlands

6 ² Institute of Earth Sciences, University of Graz, NAWI Graz, Heinrichstraße 26, 8010 Graz, Austria

7 *Correspondence to:* Stefanie Kaboth (S.Kaboth@uu.nl)

8 **Abstract.** Gaining insights into the evolution of Mediterranean Outflow Water (MOW) during the Early Pleistocene climate
9 transition has been so far hampered by the lack of available paleoclimatic archives. Here we present the first benthic
10 foraminifera stable oxygen and carbon isotope records and grain-size data from IODP Expedition 339 Site U1389 presently
11 located within the upper core of the MOW in the Gulf of Cadiz for the time interval between 2.6 and 1.8 Ma. A comparison
12 with an intermediate water mass record from the Mediterranean Sea strongly suggest an active MOW supplying Site U1389
13 on glacial-interglacial timescales during the Early Pleistocene. We also find indication that the increasing presence of MOW
14 in the Gulf of Cadiz during the investigated time interval aligns with the progressive northward protrusion of Mediterranean
15 sourced intermediate water masses into the North Atlantic, possibly modulating the intensification of the North Atlantic
16 Meridional Overturning Circulation at the same time. Additionally, our results suggest that MOW flow strength was already
17 governed by precession and semi-precession cyclicity during the Early Pleistocene against the background of glacial-
18 interglacial variability dominated by the obliquity cycle of Earth's inclination axis.

19

20 *Keywords:* Mediterranean Outflow, Early Pleistocene, Atlantic Meridional Overturning Circulation, Sapropel

21 1 Introduction

22 The Mediterranean Outflow Water (MOW) is a distinct hydrographic feature at intermediate water depths in the Gulf of
23 Cadiz, distinguished from other ambient North Atlantic water masses by its warm and saline character (Ambar and Howe,
24 1979; Bryden et al., 1994; Bryden and Stommel, 1984). In the modern hydro-climatic setting of the Mediterranean Sea the
25 MOW is predominately sourced by Levantine Intermediate Water (~70%), formed in the Eastern Mediterranean Basin, and
26 variable parts of Western Mediterranean Deep Water (WMDW) originating in the Alboran and Tyrrhenian Sea (Millot,
27 2014, 2009; Millot et al., 2006). After exiting the Strait of Gibraltar, the MOW plume cascades down the continental slope
28 due to its increased density (Ambar and Howe, 1979; Hernandez-Molina et al., 2014a; Hernández-Molina et al., 2006;
29 Mulder et al., 2006). In the Gulf of Cadiz, MOW follows the topography of the continental shelf in two major flow cores at



30 800-1400 m water depth (lower MOW core), and 500-700 m water depth including our study area (upper MOW core, Fig.1)
31 (Baringer and Price, 1997; Borenäs et al., 2002; Hernández-Molina et al., 2013). After exiting the Gulf of Cadiz, most of
32 MOW flows north along the European continental margin until it mixes with the North Atlantic Current at Rockall Plateau
33 (Hernandez-Molina et al., 2014b).

34 Beyond the Mediterranean region, MOW has been acknowledged as an important modulator of the North Atlantic salt
35 budget with previous research suggesting that the absence of MOW may reduce Atlantic Meridional Overturning Circulation
36 (AMOC) by as much as 15% compared to modern (Rogerson et al., 2006). Despite its potential cosmopolitan significance
37 the paleoceanographic history of MOW has so far been only studied for the Pliocene (Khelifi et al., 2009; Khélfifi et al.,
38 2014), and during the last climatic cycle (Bahr et al., 2015; Kaboth et al., 2016; Llave et al., 2006; Schönfeld, 2002;
39 Schönfeld and Zahn, 2000; Toucanne et al., 2007; Voelker et al., 2006). In this light, the reconstruction of MOW variability
40 might be particularly interesting in the broader view of the Pliocene-Pleistocene climate transition. The early Pleistocene
41 period spans the transition from the preceding Pliocene climate optimum with limited ice sheets in the Northern Hemisphere
42 to the cooler Middle and Late Pleistocene climate with rapidly developing continental ice growth in both hemispheres
43 (Raymo et al., 1992; Shackleton and Hall, 1984). Throughout the Early Pleistocene, however, an interruption of the long-
44 term Northern Hemisphere ice volume increase can be observed in concert with a sea-surface temperature stabilization in the
45 high latitude North Atlantic cooling trend (Bell et al., 2015). It was suggested that these changes relate to an increase in
46 AMOC strength, and in extension, an increase in northward heat transport (Bell et al., 2015).

47 Here we elaborate on the possible role of MOW on North Atlantic Paleoceanographic changes during the early Pleistocene
48 climate transition by investigating the benthic foraminifera stable oxygen and carbon isotopes and grain-sizes from IODP
49 339 Site U1389, located on the upper slope of the Gulf of Cadiz (see Fig. 1) for two time intervals: 2.6 and 2.4 Ma and 2.1
50 and 1.8 Ma. We have compared our new data with benthic stable isotope record of the Singa/Vrica sections on Calabria
51 (Italy), representing the intermediate water mass endmember of the Mediterranean Sea (Lourens et al., 1996; unpublished
52 data) that serves as a reference for the source region of MOW during the Early Pleistocene (Fig. 1). Our results bridge the
53 gap in our understanding of MOW variability between the wider researched Pliocene and Late Pleistocene. We aim to shed
54 new light on MOW variability during the Early Pleistocene by analysing hydrographic changes within the Mediterranean
55 source region, investigating the low-latitude control of MOW against the background of dominant obliquity controlled
56 glacial-interglacial cyclicity and documenting the potential influence of MOW variability on long-term climatic oscillations
57 in the North Atlantic.

58 **2 Material & Methods**

59 **2.1 Site U1389**

60 Integrated Ocean Drilling Program (IODP) Site U1389 (36°25.515'N; 7°16.683'W) was drilled in December 2011 and
61 January 2012 during Expedition 339 (Stow et al., 2013). It is located on the southern Iberian Margin ~90 km west of the city



62 of Cadiz and perched on the northwest side of the Guadalquivir diapiric ridge in 644 m water depth (Fig. 1). At present,
63 IODP Site U1389 is directly influenced by the upper MOW core (Hernández-Molina et al., 2013; Stow et al., 2002, 2013).
64 For the present study we analysed 423 samples from Site U1389 Hole E which cover the Early Pleistocene (2.6 to 1.8 Ma)
65 time interval at 30 cm intervals between 549.8 to 706.35 mbsf. An expanded hiatus at Hole U1389E between 2.1 and 2.4 Ma
66 (~622-644 mbsf) has been initially related to a phase of highly active MOW (Hernández-Molina et al., 2013; Stow et al.,
67 2013). However, more recent findings link this compressional event to tectonically invoked erosion (Hernández-Molina et
68 al., 2015). As a consequence we present the data split in two intervals (Interval I: 2.6-2.4 Myr and II: 2.1 to 1.8 Myr).

69 2.2 Stable isotope measurements and interspecies correction

70 The freeze-dried sediment samples were wet sieved into three fractions (>150 μm , >63 μm and >38 μm), and their residues
71 oven dried at 40°C. Stable oxygen ($\delta^{18}\text{O}$) and carbon ($\delta^{13}\text{C}$) isotope analyses were carried out on 4 to 6 specimens of the
72 epifaunal living foraminiferal species *Planulina ariminensis* and *Cibicides ungerianus* from the >150 μm size fraction. All
73 selected specimens were crushed, sonicated in ethanol, and dried at 35°C. Stable isotope analyses were carried out on a
74 CARBO-KIEL automated carbonate preparation device linked to a Thermo-Finnigan MAT253 mass spectrometer at Utrecht
75 University. The precision of the measurements is $\pm 0.08\text{‰}$ for $\delta^{18}\text{O}$ and ± 0.03 for $\delta^{13}\text{C}$. The results were calibrated using the
76 international standard NBS-19, and the in-house standard NAXOS. Isotopic values are reported in standard delta notation (δ)
77 relative to the Vienna Pee Dee Belemnite (VPDB).

78 *P. ariminensis* was absent in 100 samples; resulting gaps were filled with *C. ungerianus* values corrected for interspecies
79 isotopic offsets. The calculation of the interspecies offset is based on 62 paired isotope measurements of both benthic
80 species. The $\delta^{18}\text{O}$ interspecies offset was determined by applying a least square linear regression equation (Fig. 2). The
81 Pearson correlation coefficient (R^2) between both species shows high correlation of 0.79 for $\delta^{18}\text{O}$. The calculated slope of
82 this relationship is ~ 0.97 with an intercept of $+0.10\text{‰}$ between *P. ariminensis* and *C. ungerianus*.

83 In contrast, the $\delta^{13}\text{C}$ correlation was insignificant with R^2 of 0.02 between the two benthic species (Fig. 2). Therefore, we
84 only present the $\delta^{13}\text{C}$ of *P. ariminensis*, considered a valuable basis for $\delta^{13}\text{C}$ studies of the paleo-hydrography of the MOW
85 (Zahn et al., 1987).

86 2.3 Grain-size analyses

87 The stable isotope sample preparation was used to obtain weight percentages (wt.-%) of the grain-size fractions >150 μm ,
88 150-63 μm , 63-38 μm and <38 μm for the investigated samples were obtained during sample preparation for isotope
89 analyses. We concentrate on the grain-size fraction between 63-150 μm which has been used previously as indicator for flow
90 strength changes in the Gulf of Cadiz attributed to MOW variability (Rogerson et al., 2005). Even though untreated weight
91 percentages hold a bias it has been shown for the last climatic cycle that weight percentages mirror major peaks in Zr/Al
92 records, considered a reliable recorder of MOW flow strength variability (Bahr et al., 2014), and thus can be used to trace
93 patterns of MOW flow strength variability (Kaboth et al., 2016).



94 2.4 Chronology

95 Primary age constraints are based on paleomagnetic and biostratigraphic tie points as listed in Table 1. The secondary age
96 model follows the visual correlation of the benthic $\delta^{18}\text{O}$ record at Site U1389 to the benthic $\delta^{18}\text{O}$ “MedSea” stack of Lourens
97 et al. (unpublished data) within the investigated time period. The MedSea stack is based on the benthic *C. ungerianus* $\delta^{18}\text{O}$
98 values from the Singa and Vrica sections located in Calabria, Italy derived from the same samples used for the planktic $\delta^{18}\text{O}$
99 record in Lourens et al., (1996a, pers. comm.). The stable isotope measurements for the MedSea stack were carried
100 analogous the protocol described in section 2.2 (Lourens 2016, pers. comm.) The *C. ungerianus* values of the MedSea stack
101 were adjusted to the *P. ariminensis* based $\delta^{18}\text{O}$ record at Site U1389 by applying the interspecies correction equation cited
102 under section 2.2. The Mediterranean Sea stack $\delta^{18}\text{O}$ time series is based on tuning sapropel midpoints to La2004 65° N
103 summer insolation maxima, including a 3-kyr time lag (Lourens, 2004). Monitoring of the sedimentation rate was done to
104 control viability of secondary age model. The designation of MIS stages follows the MedSea stack chronology (Lourens,
105 2004). The respective tie points of the secondary age model are listed in Table 2.

106 2.5 Spectral Analysis

107 Spectral analysis was performed to test for statistically significant cycles with respect to orbital parameters. For analysis of
108 orbital periodicities, the non-constantly sampled time series were analysed by a Multi Taper Method using the program
109 REDFIT (Schulz and Mudelsee, 2002).

110 3 Results

111 3.1 Age model & Sedimentation rates

112 The two studied intervals of the Site U1389 $\delta^{18}\text{O}$ record exhibit similar glacial-interglacial variability as present in MedSea
113 stack throughout the Early Pleistocene. The estimated mean sedimentation rate for both intervals is ~ 0.30 m/kyr (Fig. 3)
114 which is similar to the sedimentation rate of ~ 0.25 to ~ 0.30 m/kyr that has been calculated from shipboard stratigraphy for
115 the past 3.2 Myr (Hernández-Molina et al., 2013; Stow et al., 2013). A doubling or tripling of the sedimentation rate
116 coincides with transition of MIS 101 to MIS 100 and interglacials MIS 99 and MIS 97 in Interval I, and \sim MIS 68 in Interval
117 II. Condensed sections with low sedimentation rates of ~ 0.1 m/kyr correlate with the transition between MIS 98 to MIS 97
118 and MIS 95 in Interval I, and MIS 78 to MIS 75 in Interval II, respectively.

119 3.2 Stable oxygen and carbon isotopes

120 The comparison between both intervals of the $\delta^{18}\text{O}$ record at Site U1389 with the benthic $\delta^{18}\text{O}$ MedSea stack is shown in
121 Figure 4. In Interval I, lightest values of 1.17 and 1.22 ‰ coincide with interglacials MIS 103 and 101, and the strongest
122 glacial enrichment in $\delta^{18}\text{O}$ (2.69 ‰) coincides with MIS 100. Transitional depletion is on average 0.97 ‰ with highest



123 values (1.29 ‰) in the interval between MIS 101 and 100 (see Fig. 4). In Interval II, the lightest values coincide with MIS 73
124 (1.36 ‰) whereas the strongest glacial $\delta^{18}\text{O}$ enrichment can be observed during MIS 78, 72 and 68 with 2.47 ‰, 2.42 ‰ and
125 2.69 ‰, respectively (see Fig. 4). Transitional depletion is on average 0.82 ‰ with highest values (1.06 ‰ and 1.19 ‰) in
126 the interval between MIS 73 and 72, and the transition from MIS 69 to MIS 68. Pronounced amplitude offsets between the
127 $\delta^{18}\text{O}$ signal of Site U1389 and MedSea are visible in both intervals but especially during MIS 103, 102, 77, 75 and 67 (Fig.
128 4). These perturbations are of the order of up to ~ 0.5 ‰ (e.g. MIS 75).

129 The comparison between both intervals of the $\delta^{13}\text{C}$ record at Site U1389 with the $\delta^{13}\text{C}$ MedSea stack is shown in Figure 4.
130 During Interval I, lightest values of 0.27 and 0.32 ‰ coincide with MIS 101 and 100, and the heaviest values (~ -1.27 ‰)
131 coincide with the transition of MIS 102 to MIS 101, MIS 100, and the transition between MIS 99 to MIS 98. In Interval II,
132 the lightest values correspond to MIS 74 (-0.02 ‰) and the transition between MIS 68 and 67 (-0.06 ‰). The heaviest $\delta^{13}\text{C}$
133 values coincide with MIS 71 (1.56 ‰).

134 3.3 Grain-size

135 The mean grain-size values (63-150 μm) for both investigated intervals are ~ 8.0 % -wt. Highest values of both investigated
136 intervals of up to ~ 60 % -wt. are correlated with MIS 100 and 77 (Fig. 4). The grain-size variability is seemingly not related
137 to glacial-interglacial variability as a clear response of the grain-size to the variability of $\delta^{18}\text{O}$ records at Site U1389 cannot
138 be observed.

139 3.4 Spectral analyses

140 The grain-size records of Interval I and II at Site U1389 exhibit significance (80% to 90%) variance in the precession (~ 23
141 kyr) and semi-precession (~ 11 kyr) frequency band (Fig. 5). The obliquity signal is insignificant in both investigated
142 intervals.

143 4 Discussion

144 4.1 Glacial-Interglacial MOW variability at Site U1389 during the Early Pleistocene

145 Site U1389 reveals $\delta^{18}\text{O}$ values similar to the MedSea stack during Interval I (2.6-2.4 Ma) and Interval II (2.1-1.8 Ma),
146 which emphasize the direct influence of intermediate Mediterranean water masses on MOW (Fig. 4). This suggests that
147 MOW formation during the Early Pleistocene was similar to modern conditions where MOW originates largely from
148 intermediate water masses such as the Levantine Intermediate Water (Millet, 2009, 2014; Millet et al., 2006).

149 The $\delta^{18}\text{O}$ difference between Site U1389 and the Mediterranean Sea is small during glacial periods in both investigated
150 intervals, suggesting that Site U1389 bathed in MOW during these colder climatic conditions throughout the early
151 Pleistocene time interval (Fig. 4). This is particularly interesting in light of the proposed vertical shift of the MOW flow path
152 during glacial periods of the Late Pleistocene fostered by the increased density of the outflowing Mediterranean water



153 masses (Kaboth et al., 2015; Lofi et al., 2015; Toucanne et al., 2007b; Voelker et al., 2006; Rogerson et al., 2005; Schönfeld
154 and Zahn, 2002). This suggests that Site U1389 was not subjected to major glacial-interglacial induced flow path changes
155 during the early Pleistocene, possibly due to its deeper and relatively proximal location to the Strait of Gibraltar, placing it
156 more into the general flow path of upper MOW. These results confirm the inferences derived from Site U1389 of the Late
157 Pleistocene interval where MOW activity was also shown to be largely unaffected by glacial-interglacial variability but
158 instead predominately influenced by insolation driven hydro-climatic changes of its Mediterranean source region (Bahr et
159 al., 2015).

160 In contrast, the interglacial periods of both intervals show a small but relative depletion in the Mediterranean Sea compared
161 to the $\delta^{18}\text{O}$ signal at Site U1389 which might reflect relatively higher temperatures or lower salinity of the intermediate
162 Mediterranean Sea waters with respect to the MOWs during interglacial periods. The strongest intervals of relative $\delta^{18}\text{O}$
163 depletion throughout both investigated time periods correlate with MIS 103, 102, MIS 75 and MIS 67 characterized by a
164 depletion of up to $\sim 0.5\%$ in the Mediterranean Sea compared to Site U1389. This shift might correspond to a freshening of
165 the Mediterranean Sea intermediate water column during sapropel formation and a consequently reduction of MOW
166 influence at Site U1389 (Rogerson et al., 2012). In case of MIS 102 and 67 sapropels have been documented in the Eastern
167 Mediterranean Sea basin but not for MIS 75 (Emeis et al., 2000; Lourens, 2004; Lourens et al., 1992, 1996a).

168 During Interval II, the generally heavier $\delta^{13}\text{C}$ values at U1389 are close to those of the Mediterranean Sea values inferring
169 that MOW was in fact the predominant source of bottom water at Site U1389 between 1.8 and 2.1 Ma. In contrast, the older
170 Interval I is characterized by a slightly increased $\delta^{13}\text{C}$ gradient between Site U1389 and the Mediterranean Sea suggesting a
171 generally larger contribution of ambient North Atlantic water masses carrying a lighter $\delta^{13}\text{C}$ signal to the site. This could
172 indicate a more vigorous MOW or that during Interval I the MOW flow core was less proximal than during Interval II. The
173 later argument seems to be supported by the grain-size and its variability, as Interval II shows a $\sim 10\%$ decrease in mean and
174 amplitude relative to Interval I (Fig. 4). This would suggest that during Interval I Site U1389 was less proximal to the flow
175 core albeit more sensitive to flow strength changes whereas during Interval II the MOW plume has settled upon Site U1389.
176 This is further supported by findings from seismic records in the Gulf of Cadiz that also suggest that at ~ 2.1 Ma the present
177 day circulation established (Hernandez-Molina et al., 2014b)

178 A distinct increase in the $\delta^{13}\text{C}$ gradient can be seen during MIS 96, which may document a particular strong MOW activity.
179 However, the sample resolution during MIS 96 and the subsequent MIS 95 is relatively low so that increase in the $\delta^{13}\text{C}$
180 gradient remains ambiguous. The onset of the subsequent hiatus which has been argued to represent depositional erosion due
181 to increased bottom current activity of the MOW could argue for a strong intensification of MOW activity (Hernandez-
182 Molina et al., 2014b).



183 **4.2 Precession control on MOW strength during the Early Pleistocene: Similarities to Late Pleistocene MOW**
184 **behaviour?**

185 Untreated grain-size weight percentages can only give an indication for patterns in flow strength (Kaboth et al., 2016). For
186 the two investigated intervals we find that the 63-150 μm fraction variability is seemingly modulated by a ~ 23 kyr pacing
187 (Fig. 4). This relationship is evident in the power spectrum of the grain-size data which yields for both intervals a dominance
188 in the precession frequency band (~ 23 kyr); more prominently in the younger than in the older interval (Fig. 5). This
189 suggests that the flow strength of MOW was probably directly modulated by precession during the Early Pleistocene,
190 aligning with previous findings based on Zr/Al ratios at Site U1389 from the Late Pleistocene (Bahr et al., 2015). For the late
191 Pleistocene, an inverse relationship was found between precession and MOW dynamics (Bahr et al., 2015; Kaboth et al.,
192 2016). During periods of increased summer insolation at the time of precession minima, the monsoonal rain belts expand
193 northward causing an increase of freshwater discharge by the river Nile (e.g. Rohling et al., 2015; Rossignol-Strick, 1985,
194 1983). This effectively impedes intermediate water mass formation in the Eastern Mediterranean, thereby suppressing MOW
195 production. From the correlation of the filtered ~ 23 kyr signal to the grain-size variability at site U1389 a similar relationship
196 already existed during both investigated intervals of the Early Pleistocene (Fig. 4). We also find significant semi-precession
197 (~ 11 kyr) influence indicative for a primarily low-latitude response argued to originate in the tropics (Rutherford and
198 D'Hondt, 2000; de Winter et al., 2014).

199 The $\delta^{18}\text{O}$ signal comparison of Site U1389 and the MedSea stack is also particular interesting in the context of sapropel
200 formation, as the MedSea stack due to its intermediate paleo-water depth was sensitive to freshwater induced changes in the
201 intermediate water composition. A substantial freshening of the intermediate water masses in the Mediterranean Sea can be
202 inferred from the strongly depleted $\delta^{18}\text{O}$ values during MIS 103, 102, 77, 75 and 67 relative to Site U1389 (Fig. 4). The
203 potentially reduced MOW supply at Site U1389 at the same time would increase the isotopic gradient between both
204 locations, as Site U1389 could be affected by more open ocean conditions. However, despite the low sample resolution, this
205 seems not a persistent relationship throughout both investigated intervals. For the Holocene S1, the proposed reduction in
206 MOW has been documented by the absence of sandy contourite layers from the middle slope of the Gulf of Cadiz indicating
207 a sudden reduction in flow strength and sediment delivery by the MOW (Toucanne et al., 2007; Voelker et al., 2006). The
208 grain-size values throughout both investigated intervals at Site U1389 are typically low during sapropel formation supporting
209 the findings from the middle and upper slope during the Late Pleistocene (Kaboth et al., 2016). However, the grain-size is
210 seemingly increased during the sapropels deposited in the Eastern Mediterranean Sea at ~ 1.92 and 1.85 Myrs (Fig. 4). This
211 in-phase behaviour could potentially be a tuning artefact or relate to the fact that numerical model simulations imply that
212 remnant thermal riven overturning circulation still occurs throughout the most extreme freshening events in the eastern
213 Mediterranean Sea (Myers, 2002). This would imply that during the sapropel formation at ~ 1.92 and 1.85 Myrs MOW was
214 potentially still active at Site U1389.



215 4.3 Did MOW contribute to the Early Pleistocene climate transition?

216 Between ~2.8 and 2.4 Myrs (Interval I) occurrences of *Neogloboquadrina atlantica* (sin), an extinct polar species, were
217 reported in the Mediterranean Sea during glacial periods suggesting the intrusion of colder water masses into the
218 Mediterranean basin (Becker et al., 2005; Lourens and Hilgen, 1997; Zachariasse et al., 1990). We also find *N. atlantica*
219 (sin) present during glacial periods of Interval I (Fig. 4), confirming a more southern delineation of transitional and subpolar
220 water masses during glacial periods of the Early Pleistocene than in recent setting (Voelker et al., 2015). This latitudinal shift
221 might occurred in concert with a more sluggish AMOC at least during the glacial periods if not throughout the whole time
222 interval (Bell et al., 2015). Colder and more arid background conditions in the Mediterranean Sea could foster a stronger
223 MOW analogous to cold spells related to Heinrich Events throughout the last climatic cycle (Bahr et al., 2014, 2015; Kaboth
224 et al., 2016). An intensification of MOW during Interval I would align with the increased $\delta^{13}\text{C}$ gradient between Site U1389
225 and the Mediterranean Sea suggesting a more vigorous MOW which is also reflected by higher grain-size amplitudes
226 compared to Interval II (Fig. 4). Our data, however, do not extend further back in time to test whether these conditions
227 coincides with the proposed steady increase of MOW activity in the Gulf of Cadiz since 3.2 Ma as inferred from natural
228 gamma ray logs and seismic profiles (Hernández-Molina et al., 2015), and with the arrival of Mediterranean sourced
229 intermediate water mass at North Atlantic Sites DSDP 548 and 552 and ODP 982 from ~3.6 onwards (Khélifi et al., 2014;
230 Loubere, 1987). This northward protrusion of warm and saline MOW towards high-latitude deep-water convection hot spots
231 is considered an important modulator of the North Atlantic salt budget (Bahr et al., 2015; Rogerson et al., 2006; Voelker et
232 al., 2006). We suggest that steady contributions of MOW throughout Interval I supplied continuously salt into the North
233 Atlantic and potentially preconditioned the strong AMOC activity phase starting at ~2.4 Ma (Bell et al., 2015) when a
234 tipping point was reached. The Early Pleistocene MOW might therefore have acted as a positive climatic feedback
235 mechanism against the background of increasingly colder temperatures (Fig. 4). This stands in contrast to the warm Pliocene
236 setting where it was proposed that MOW contributions to the North Atlantic did not have a significant influence on the
237 AMOC (Khélifi et al., 2014).

238 The intensification of the AMOC is also in concert with the disappearance of *N. atlantica* (sin) in the Mediterranean Sea and
239 the North Atlantic up to at least 52°N after ~2.4 Ma (Lourens and Hilgen, 1997; Weaver and Clement, 1987). This suggests
240 the reduction in southward protrusion of colder water masses and hence the *N. atlantica* extinction, and a return to a warmer
241 background climate in the Mediterranean region during glacial periods (Lourens, 2008).

242 The increased AMOC activity is documented by the North Atlantic SST record of Site ODP 982 displaying a plateau starting
243 at ~2.4 Ma indicating more steady climate conditions (Fig. 4), and a stagnation in Northern Hemisphere ice sheet growth
244 (Bell et al., 2015; Lawrence et al., 2009). Coinciding with this stabilization of North Atlantic SSTs is a cooling in the South
245 Atlantic attributed to a northward piracy of the tropical warmer water pool by a strong AMOC and implying an active
246 interhemispheric climatic seesaw at that time (Patterson et al., 2014; Etourneau et al., 2010). Despite the lack of direct data at
247 Site U1389 between the 2.4 to 2.1 Ma interval, seismic records from the Gulf of Cadiz suggest that the hiatus represents a



248 depositional erosion feature caused by intensified bottom current activity, and hence strong MOW flow (Hernandez-Molina
249 et al., 2014b). This would align with the continuous strong AMOC activity in the North Atlantic (Bell et al., 2015).
250 From the reduction of the $\delta^{18}\text{O}$ and $\delta^{13}\text{C}$ gradient between Site U1389 and the MedSea stack (Fig. 4), it appears that after
251 ~ 2.1 Ma MOW settled and upon Site U1389 (Fig. 4). The reduction in grain-size might also imply more stable MOW
252 behaviour whereas during the transitional phase of the older Interval I MOW was probably more erratic, indicated by the
253 high grain-size variability and the increased $\delta^{13}\text{C}$ gradient (Fig. 4). Unfortunately, we lack data beyond ~ 2.5 Ma from ODP
254 Sites 549, 552 and 982 to further trace the temporal MOW influence in the high-latitude North Atlantic throughout Interval
255 II but it stands to reason that continued MOW contributions also during Interval II might have contributed to the sustained
256 AMOC activity.

257 **5 Conclusions**

258 Based on our results, the supply of MOW to Site U1389 was already established during the Early Pleistocene and not limited
259 to Late Pleistocene climate conditions. In addition, we find indication that the MOW flow strength might have been
260 modulated by precession superimposed on glacial-interglacial change, this aligns with findings from the Late Pleistocene at
261 Site U1389 and suggests that Site U1389 is a true recorder of MOW variability also throughout Early Pleistocene. In the
262 broader view of the Early Pleistocene climate transition we find indication that increased MOW might have contributed to
263 the increased AMOC phases starting from 2.4 Ma, and thus influencing North Atlantic oceanic heat transport.

264 **Data availability**

265 The data related to this manuscript is already stored in PANGEA and placed under moratorium. After a final decision has
266 been made about the publication of this manuscript the data will made publicly accessible.

267 **Author contribution**

268 S. Kaboth conducted the measurements, data analyses, and prepared the manuscript with contributions from P. Grunert and
269 L. Lourens. Additionally, L. Lourens and P. Grunert provide financial support to this submission.

270 **Competing interests**

271 The authors declare that they have no conflict of interest.



272 **Disclaimer**

273 Figure 1 (Study area) is a modified version of an already published figure (Hernández-Molina et al., 2013; Stow et al., 2013).
274 The figure is used under creative commons Attribution 3.0 unported licence.

275 **Acknowledgements**

276 We acknowledge the Integrated Ocean Drilling Program (IODP) for providing the samples used in this study as well as A.
277 van Dijk at Utrecht University for analytical support. This research was funded by NWO-ALW grant (project number
278 865.10.001) to Lucas J. Lourens and contributions from project P25831-N29 of the Austrian Science Fund (FWF).

279 **References**

- 280 Ambar, I. and Howe, M. R.: Observations of the mediterranean outflow—II the deep circulation in the vicinity of the gulf of
281 cadiz, *Deep Sea Res. Part A. Oceanogr. Res. Pap.*, 26(5), 555–568, doi:10.1016/0198-0149(79)90096-7, 1979.
282
- 283 Bahr, A., Jiménez-Espejo, F. J., Kolasinac, N., Grunert, P., Hernández-Molina, F. J., Röhl, U., Voelker, A. H. L., Escutia, C.,
284 Stow, D. A. V., Hodell, D. and Alvarez-Zarikian, C. A.: Deciphering bottom current velocity and paleoclimate signals from
285 contourite deposits in the Gulf of Cadiz during the last 140kyr: an inorganic geochemical approach, *Geochemistry, Geophys.*
286 *Geosystems*, 15(8), 3145–3160, doi:10.1002/2014GC005356, 2014.
287
- 288 Bahr, A., Kaboth, S., Jiménez-Espejo, F. J., Sierro, F. J., Voelker, A. H. L., Lourens, L., Röhl, U., Reichart, G. J., Escutia,
289 C., Hernández-Molina, F. J., Pross, J. and Friedrich, O.: Persistent monsoonal forcing of Mediterranean Outflow Water
290 dynamics during the late Pleistocene, *Geology*, 43(11), 951–954, doi:10.1130/G37013.1, 2015.
- 291 Baringer, M. O. and Price, J. F.: Mixing and Spreading of the Mediterranean Outflow, *J. Phys. Oceanogr.*, 27, 1654–1677,
292 doi:10.1175/1520-0485(1997)027<1654:MASOTM>2.0.CO;2, 1997.
293
- 294 Becker, J., Lourens, L. J., Hilgen, F. J., van der Laan, E., Kouwenhoven, T. J. and Reichart, G.-J.: Late Pliocene climate
295 variability on Milankovitch to millennial time scales: A high-resolution study of MIS100 from the Mediterranean,
296 *Palaeogeogr. Palaeoclimatol. Palaeoecol.*, 228(3–4), 338–360, doi:10.1016/j.palaeo.2005.06.020, 2005.
297
- 298 Bell, D. B., Jung, S. J. A. and Kroon, D.: The Plio-Pleistocene development of Atlantic deep-water circulation and its
299 influence on climate trends, *Quat. Sci. Rev.*, 123, 265–282, doi:10.1016/j.quascirev.2015.06.026, 2015.
300



- 301 Borenäs, K. M., Wåhlin, A. K., Ambar, I. and Serra, N.: The Mediterranean outflow splitting—a comparison between
302 theoretical models and CANIGO data, *Deep Sea Res. Part II Top. Stud. Oceanogr.*, 49, 4195–4205, doi:10.1016/S0967-
303 0645(02)00150-9, 2002.
- 304
- 305 Bryden, H. L. and Stommel, H. M.: Limiting processes that determine basic features of the circulation in the Mediterranean
306 Sea, *Oceanol. Acta*, 7(3), 289–296, 1984.
- 307
- 308 Bryden, H. L., Candela, J. and Kinder, T. H.: Exchange through the Strait of Gibraltar, *Prog. Oceanogr.*, 33, 201–248,
309 doi:10.1016/0079-6611(94)90028-0, 1994.
- 310
- 311 Emeis, K.-C., Sakamoto, T., Wehausen, R. and Brumsack, H.-J.: The sapropel record of the eastern Mediterranean Sea —
312 results of Ocean Drilling Program Leg 160, *Palaeogeogr. Palaeoclimatol. Palaeoecol.*, 158(3–4), 371–395,
313 doi:10.1016/S0031-0182(00)00059-6, 2000.
- 314
- 315 Etourneau, J., Schneider, R., Blanz, T. and Martinez, P.: Intensification of the Walker and Hadley atmospheric circulations
316 during the Pliocene–Pleistocene climate transition, *Earth Planet. Sci. Lett.*, 297(1–2), 103–110,
317 doi:10.1016/j.epsl.2010.06.010, 2010.
- 318
- 319 Gradstein, F. M., Ogg, J. G. and Hilgen, F. J.: On The Geologic Time Scale, *Newsletters Stratigr.*, 45(2), 171–188,
320 doi:10.1127/0078-0421/2012/0020, 2012.
- 321
- 322 Hernandez-Molina, F. J., Llave, E., Preu, B., Ercilla, G., Fontan, A., Bruno, M., Serra, N., Gomiz, J. J., Brackenridge, R. E.,
323 Sierro, F. J., Stow, D. A. V., Garcia, M., Juan, C., Sandoval, N. and Arnaiz, A.: Contourite processes associated with the
324 Mediterranean Outflow Water after its exit from the Strait of Gibraltar: Global and conceptual implications, *Geology*, 42(3),
325 227–230, doi:10.1130/G35083.1, 2014a.
- 326
- 327 Hernandez-Molina, F. J., Stow, D. A. V., Alvarez-Zarikian, C. A., Acton, G., Bahr, A., Balestra, B., Ducassou, E., Flood, R.,
328 Flores, J.-A., Furota, S., Grunert, P., Hodell, D., Jimenez-Espejo, F., Kim, J. K., Krissek, L., Kuroda, J., Li, B., Llave, E.,
329 Lofi, J., Lourens, L., Miller, M., Nanayama, F., Nishida, N., Richter, C., Roque, C., Pereira, H., Sanchez Goni, M. F., Sierro,
330 F. J., Singh, A. D., Sloss, C., Takashimizu, Y., Tzanova, A., Voelker, A., Williams, T. and Xuan, C.: Onset of Mediterranean
331 outflow into the North Atlantic, *Science* (80-.), 344(6189), 1244–1250, doi:10.1126/science.1251306, 2014b.
- 332
- 333 Hernández-Molina, F. J., Llave, E., Stow, D. A. V., García, M., Somoza, L., Vázquez, J. T., Lobo, F. J., Maestro, A., Díaz
334 del Río, V., León, R., Medialdea, T. and Gardner, J.: The contourite depositional system of the Gulf of Cádiz: A sedimentary



- 335 model related to the bottom current activity of the Mediterranean outflow water and its interaction with the continental
336 margin, *Deep Sea Res. Part II Top. Stud. Oceanogr.*, 53(11–13), 1420–1463, doi:10.1016/j.dsr2.2006.04.016, 2006.
337
- 338 Hernández-Molina, F. J., Stow, D., Alvarez-Zarikian, C., Acton, G., Bahr, A., Balestra, B., Ducassou, E., Flood, R., Flores,
339 J. A., Furota, S., Grunert, P., Hodell, D., Jimenez-Espejo, F., Kim, J. K., Krissek, L., Kuroda, J., Li, B., Llave, E., Lofi, J.,
340 Lourens, L., Miller, M., Nanayama, F., Nishida, N., Richter, C., Roque, C., Pereira, H., Goñi Fernanda Sanchez, M., Sierro,
341 F. J., Singh, A. D., Sloss, C., Takashimizu, Y., Tzanova, A., Voelker, A., Williams, T. and Xuan, C.: IODP Expedition 339
342 in the Gulf of Cadiz and off West Iberia: Decoding the environmental significance of the Mediterranean outflow water and
343 its global influence, *Sci. Drill.*, 16, 1–11, doi:10.5194/sd-16-1-2013, 2013.
344
- 345 Hernández-Molina, F. J., Sierro, F. J., Llave, E., Roque, C., Stow, D. A. V., Williams, T., Lofi, J., Van der Schee, M.,
346 Arnáiz, A., Ledesma, S., Rosales, C., Rodríguez-Tovar, F. J., Pardo-Igúzquiza, E. and Brackenridge, R. E.: Evolution of the
347 gulf of Cadiz margin and southwest Portugal contourite depositional system: Tectonic, sedimentary and paleoceanographic
348 implications from IODP expedition 339, *Mar. Geol.*, doi:10.1016/j.margeo.2015.09.013, 2015.
349
- 350 Kaboth, S., Bahr, A., Reichert, G.-J., Jacobs, B. and Lourens, L. J.: New insights into upper MOW variability over the last
351 150kyr from IODP 339 Site U1386 in the Gulf of Cadiz, *Mar. Geol.*, 377, 136–145, doi:10.1016/j.margeo.2015.08.014,
352 2016.
353
- 354 Khelifi, N., Sarnthein, M., Andersen, N., Blanz, T., Frank, M., Garbe-Schonberg, D., Haley, B. A., Stumpf, R. and Weinelt,
355 M.: A major and long-term Pliocene intensification of the Mediterranean outflow, 3.5–3.3 Ma ago, *Geology*, 37(9), 811–814,
356 doi:10.1130/G30058A.1, 2009.
357
- 358 Khélifi, N., Sarnthein, M., Frank, M., Andersen, N. and Garbe-Schönberg, D.: Late Pliocene variations of the Mediterranean
359 outflow, *Mar. Geol.*, 357, 182–194, doi:10.1016/j.margeo.2014.07.006, 2014.
360
- 361 Lawrence, K. T., Herbert, T. D., Brown, C. M., Raymo, M. E. and Haywood, A. M.: High-amplitude variations in North
362 Atlantic sea surface temperature during the early Pliocene warm period: VARIABLE PLIOCENE NORTH ATLANTIC
363 SSTs, *Paleoceanography*, 24(2), n/a–n/a, doi:10.1029/2008PA001669, 2009.
364
- 365 Llave, E., Schönfeld, J., Hernández-Molina, F. J., Mulder, T., Somoza, L., Díaz Del Río, V. and Sánchez-Almazo, I.: High-
366 resolution stratigraphy of the Mediterranean outflow contourite system in the Gulf of Cadiz during the late Pleistocene: The
367 impact of Heinrich events, *Mar. Geol.*, 227, 241–262, doi:10.1016/j.margeo.2005.11.015, 2006.
368



- 369 Loubere, P.: Changes in mid-depth North Atlantic and Mediterranean circulation during the Late Pliocene — Isotopic and
370 sedimentological evidence, *Mar. Geol.*, 77(1–2), 15–38, doi:10.1016/0025-3227(87)90081-8, 1987.
371
- 372 Lourens, L. J.: Revised tuning of Ocean Drilling Program Site 964 and KC01B (Mediterranean) and implications for the δ^{18}
373 O, tephra, calcareous nannofossil, and geomagnetic reversal chronologies of the past 1.1 Myr: PLEISTOCENE
374 ASTRONOMICAL TIMESCALES, *Paleoceanography*, 19(3), n/a-n/a, doi:10.1029/2003PA000997, 2004.
375
- 376 Lourens, L. J.: On the Neogene-Quaternary debate, *Episodes*, 31, 239–242, 2008.
377
- 378 Lourens, L. J. and Hilgen, F. J.: Long-periodic variations in the earth’s obliquity and their relation to third-order eustatic
379 cycles and late Neogene glaciations, *Quat. Int.*, 40, 43–52, doi:10.1016/S1040-6182(96)00060-2, 1997.
380
- 381 Lourens, L. J., Hilgen, F. J., Gudjonsson, L. and Zachariasse, W. J.: Late Pliocene to early Pleistocene astronomically forced
382 sea surface productivity and temperature variations in the Mediterranean, *Mar. Micropaleontol.*, 19(1–2), 49–78,
383 doi:10.1016/0377-8398(92)90021-B, 1992.
384
- 385 Lourens, L. J., Hilgen, F. J., Raffi, I. and Vergnaud-Grazzini, C.: Early Pleistocene chronology of the Vrica Section
386 (Calabria, Italy), *Paleoceanography*, 11(6), 797–812, doi:10.1029/96PA02691, 1996a.
387
- 388 Lourens, L. J., Antonarakou, A., Hilgen, F. J., Van Hoof, A. A. M., Vergnaud-Grazzini, C. and Zachariasse, W. J.:
389 Evaluation of the Plio-Pleistocene astronomical timescale, *Paleoceanography*, 11(4), 391–413, doi:10.1029/96PA01125,
390 1996b.
391
- 392 Millot, C.: Another description of the Mediterranean Sea outflow, *Prog. Oceanogr.*, 82, 101–124,
393 doi:10.1016/j.pocean.2009.04.016, 2009.
394
- 395 Millot, C.: Heterogeneities of in- and out-flows in the Mediterranean Sea, *Prog. Oceanogr.*, 120, 254–278,
396 doi:10.1016/j.pocean.2013.09.007, 2014.
397
- 398 Millot, C., Candela, J., Fuda, J.-L. and Tber, Y.: Large warming and salinification of the Mediterranean outflow due to
399 changes in its composition, *Deep Sea Res. Part I Oceanogr. Res. Pap.*, 53(4), 656–666, doi:10.1016/j.dsr.2005.12.017, 2006.
400



- 401 Mulder, T., Lecroart, P., Hanquiez, V., Marches, E., Gonthier, E., Guedes, J.-C., Thiébot, E., Jaaidi, B., Kenyon, N., Voisset,
402 M., Perez, C., Sayago, M., Fuchey, Y. and Bujan, S.: The western part of the Gulf of Cadiz: contour currents and turbidity
403 currents interactions, *Geo-Marine Lett.*, 26(1), 31–41, doi:10.1007/s00367-005-0013-z, 2006.
- 404
- 405 Myers, P. G.: Flux-forced simulations of the paleocirculation of the Mediterranean, *Paleoceanography*, 17(1), 1009,
406 doi:10.1029/2000PA000613, 2002.
- 407
- 408 Raymo, M. E., Hodell, D. and Jansen, E.: Response of deep ocean circulation to initiation of northern hemisphere glaciation
409 (3-2 MA), *Paleoceanography*, 7(5), 645–672, doi:10.1029/92PA01609, 1992.
- 410
- 411 Rogerson, M., Rohling, E. J., Weaver, P. P. E. and Murray, J. W.: Glacial to interglacial changes in the settling depth of the
412 Mediterranean Outflow plume: CHANGES IN THE MEDITERRANEAN OUTFLOW, *Paleoceanography*, 20(3), 1–12,
413 doi:10.1029/2004PA001106, 2005.
- 414
- 415 Rogerson, M., Rohling, E. J. and Weaver, P. P. E.: Promotion of meridional overturning by Mediterranean-derived salt
416 during the last deglaciation: PROMOTION OF MERIDIONAL OVERTURNING, *Paleoceanography*, 21(4), n/a-n/a,
417 doi:10.1029/2006PA001306, 2006.
- 418
- 419 Rogerson, M., Rohling, E. J., Bigg, G. R. and Ramirez, J.: Paleoceanography of the Atlantic-Mediterranean exchange:
420 Overview and first quantitative assessment of climatic forcing, *Rev. Geophys.*, 50(2), RG2003, doi:10.1029/2011RG000376,
421 2012.
- 422
- 423 Rohling, E. J., Marino, G. and Grant, K. M.: Mediterranean climate and oceanography, and the periodic development of
424 anoxic events (sapropels), *Earth-Science Rev.*, 143, 62–97, doi:10.1016/j.earscirev.2015.01.008, 2015.
- 425 Rossignol-Strick, M.: African monsoons, an immediate climate response to orbital insolation, *Nature*, 304(5921), 46–49,
426 doi:10.1038/304046a0, 1983.
- 427
- 428 Rossignol-Strick, M.: Mediterranean Quaternary sapropels, an immediate response of the African monsoon to variation of
429 insolation, *Palaeogeogr. Palaeoclimatol. Palaeoecol.*, 49(3–4), 237–263, doi:10.1016/0031-0182(85)90056-2, 1985.
- 430 Rutherford, S. and D’Hondt, S.: Early onset and tropical forcing of 100,000-year Pleistocene glacial cycles, *Nature*,
431 408(6808), 72–75, doi:10.1038/35040533, 2000.
- 432
- 433 Schönfeld, J.: A new benthic foraminiferal proxy for near-bottom current velocities in the Gulf of Cadiz, northeastern
434 Atlantic Ocean, *Deep. Res. Part I Oceanogr. Res. Pap.*, 49, 1853–1875, doi:10.1016/S0967-0637(02)00088-2, 2002.



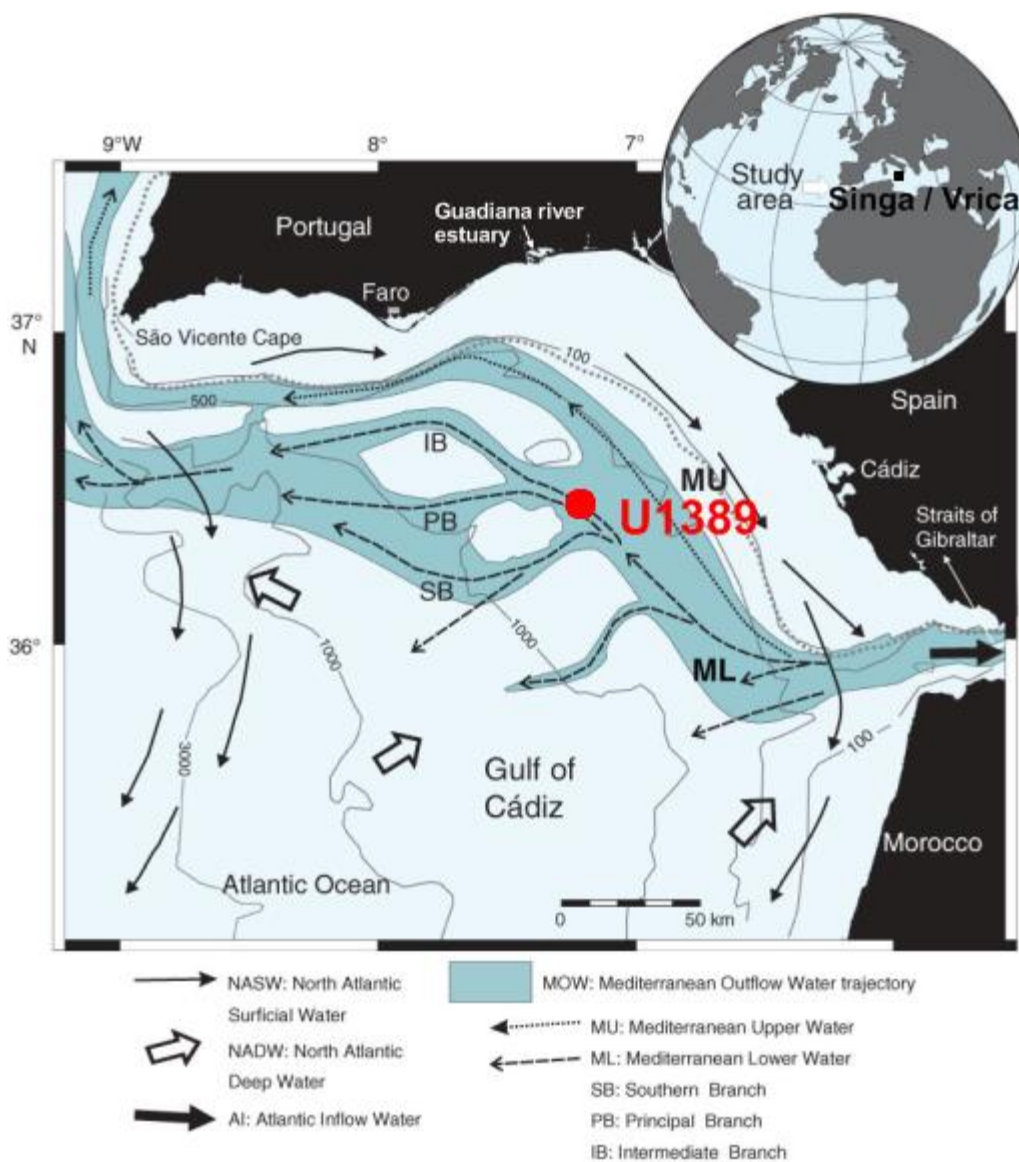
- 435
- 436 Schönfeld, J. and Zahn, R.: Late Glacial to Holocene history of the Mediterranean outflow. Evidence from benthic
437 foraminiferal assemblages and stable isotopes at the Portuguese margin, *Palaeogeogr. Palaeoclimatol. Palaeoecol.*, 159, 85–
438 111, doi:10.1016/S0031-0182(00)00035-3, 2000.
- 439
- 440 Schulz, M. and Mudelsee, M.: REDFIT: estimating red-noise spectra directly from unevenly spaced paleoclimatic time
441 series, *Comput. Geosci.*, 28(28), 421–426, 2002.
- 442
- 443 Shackleton, N. J. and Hall, M. A.: Oxygen and carbon isotope stratigraphy of the deep sea drilling project hole 552A: Plio-
444 Pleistocene glacial history, *Initial Reports DSDP*, 81, 599–609 [online] Available from:
445 <http://dx.doi.org/10.1029/2000PA000513>, 1984.
- 446
- 447 Stow, D. A. V., Faugeres, J.-C., Gonthier, E., Cremer, M., Llave, E., Hernandez-Molina, F. J., Somoza, L. and Diaz-Del-Rio,
448 V.: Faro-Albufeira drift complex, northern Gulf of Cadiz, *Geol. Soc. London, Mem.*, 22, 137–154,
449 doi:10.1144/GSL.MEM.2002.022.01.11, 2002.
- 450
- 451 Stow, D. A. V., Hernández-Molina, F. J. and Alvarez-Zarikian, C.: Expedition 339 Summary, edited by Expedition 339
452 Scientists, *Exped. 339 Summ., Proceedings of the Integrated Ocean Drilling Program(339)*,
453 doi:10.2204/iodp.proc.339.104.2013, 2013.
- 454
- 455 Toucanne, S., Mulder, T., Schönfeld, J., Hanquiez, V., Gonthier, E., Duprat, J., Cremer, M. and Zaragosi, S.: Contourites of
456 the Gulf of Cadiz: A high-resolution record of the paleocirculation of the Mediterranean outflow water during the last 50,000
457 years, *Palaeogeogr. Palaeoclimatol. Palaeoecol.*, 246, 354–366, doi:10.1016/j.palaeo.2006.10.007, 2007.
- 458
- 459 Voelker, A., Lebreiro, S., Schönfeld, J., Cacho, I., Erlenkeuser, H. and Abrantes, F.: Mediterranean outflow strengthening
460 during northern hemisphere coolings: A salt source for the glacial Atlantic?, *Earth Planet. Sci. Lett.*, 245(1–2), 39–55,
461 doi:10.1016/j.epsl.2006.03.014, 2006.
- 462
- 463 Voelker, A. H. L., Colman, A., Olack, G., Waniek, J. J. and Hodell, D.: Oxygen and hydrogen isotope signatures of
464 Northeast Atlantic water masses, *Deep Sea Res. Part II Top. Stud. Oceanogr.*, 116, 89–106, doi:10.1016/j.dsr2.2014.11.006,
465 2015.
- 466 Weaver, P.P.E and Clement, B.M.: Magnetobiostratigraphy of planktonic foraminiferal datums: Deep Sea Drilling Project
467 Leg 94, North Atlantic, vol. 94, U.S. Government Printing Office. [online] Available from:
468 http://deepseadrilling.org/94/dsdp_toc.htm (Accessed 24 May 2016), 1987.



- 469
- 470 de Winter, N. J., Zeeden, C. and Hilgen, F. J.: Low-latitude climate variability in the Heinrich frequency band of the Late
471 Cretaceous greenhouse world, *Clim. Past*, 10(3), 1001–1015, doi:10.5194/cp-10-1001-2014, 2014.
- 472
- 473 Zachariasse, W. J., Gudjonsson, L., Hilgen, F. J., Langereis, C. G., Lourens, L. J., Verhallen, P. J. J. M. and Zijderveld, J. D.
474 A.: Late Gauss to Early Matuyama invasions of *Neogloboquadrina Atlantica* in the Mediterranean and associated record of
475 climatic change, *Paleoceanography*, 5(2), 239–252, doi:10.1029/PA005i002p00239, 1990.
- 476
- 477 Zahn, R., Sarnthein, M. and Erlenkeuser, H.: Benthic isotope evidence for changes of the Mediterranean outflow during the
478 Late Quaternary, *Paleoceanography*, 2(6), 543–559, doi:10.1029/PA002i006p00543, 1987.



479

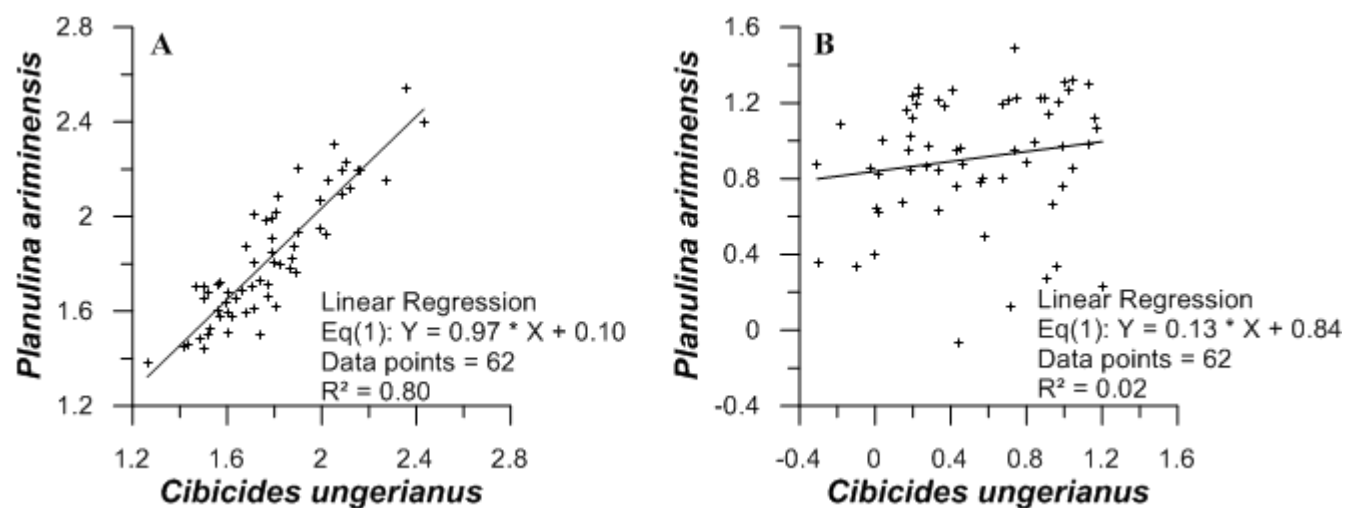


480

481 **Figure 1: Study area with illustration of modern MOW pathways modified after (Hernández-Molina et al., 2013; Stow et al.,**
 482 **2013). Site location of U1389 (red dot) and the location of the Singa/Vrica section in Italy (black dot) are marked.**



483

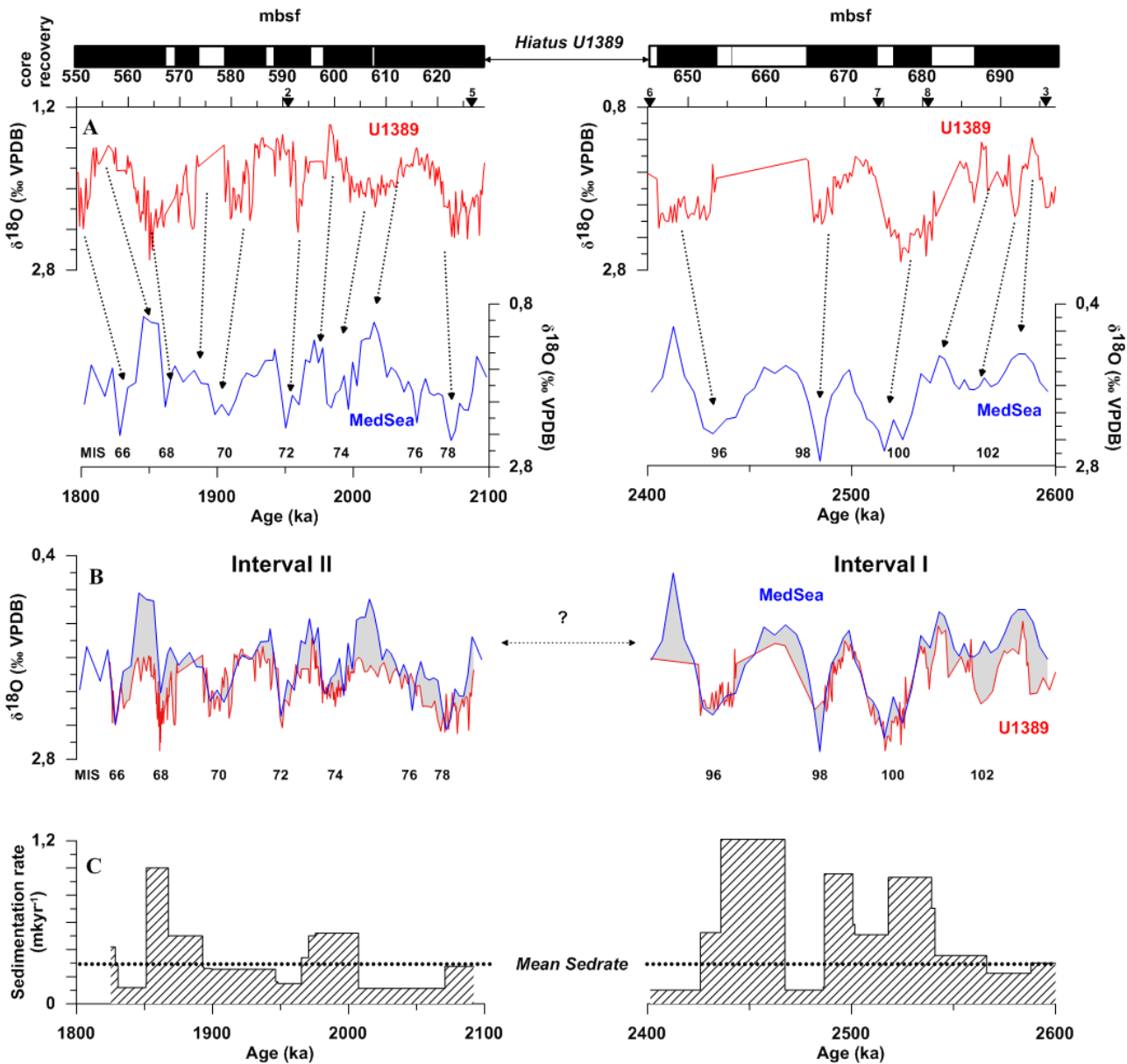


484

485 Figure 2: The $\delta^{18}\text{O}$ and $\delta^{13}\text{C}$ interspecies correlation between benthic foraminifera *Cibicides ungerianus* and *Planulina ariminensis*
486 at Site U1389. Parallel measurements were conducted throughout both investigated intervals. Linear square regression (red line)
487 equation and Pearson correlation coefficient (R^2) are shown.



488

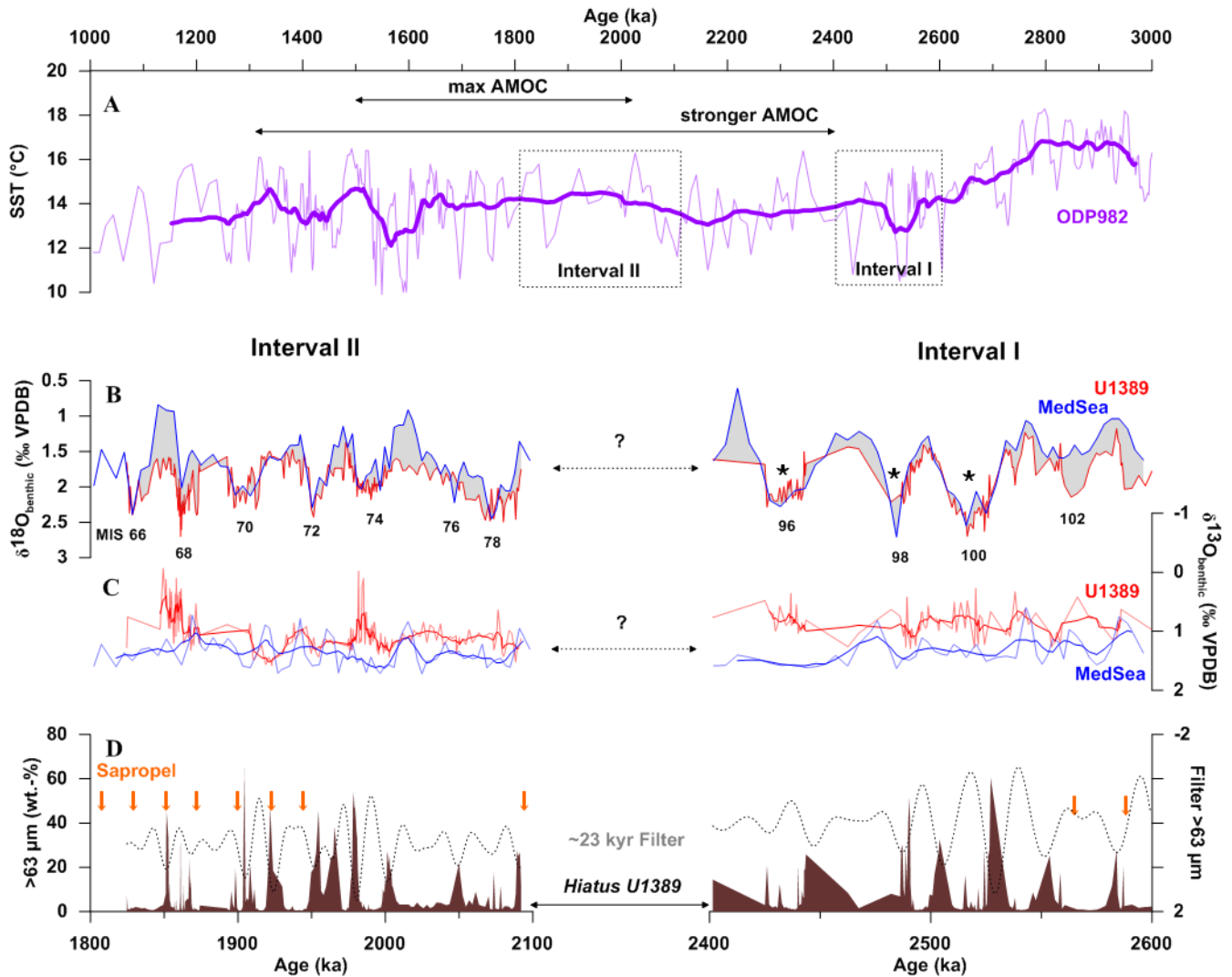


489

490 **Figure 3: Chronology of Site U1389.** Assigned marine isotope stages (MIS) follow Lourens et al. (2004). (A) Both intervals of the
 491 $\delta^{18}\text{O}$ record of Site U1389 on shipboard MCD scale correlated to the benthic $\delta^{18}\text{O}$ record of the Mediterranean Sea (MedSea
 492 stack) after Lourens et al. (1996, unpublished data). Chronostratigraphy of MedSea stack is based on tuning sapropel midpoints to
 493 La2004 65° N summer insolation (Lourens, 2004). Lines with arrows indicate selected tie points used for the age model (a full list of
 494 tie points is available in Table 2). Black triangles with numbers indicating used biostratigraphic and paleomagnetic tie points as
 495 referenced in Table 1. Black and white bar at the top represents core recovery following Hernández-Molina et al. (2013) (B)
 496 Comparison of the benthic $\delta^{18}\text{O}$ record of Site U1389 on new time scale according to our tuning, and the benthic $\delta^{18}\text{O}$ MedSea
 497 stack on its respective age model (Lourens et al. 2004) (C) Calculated sedimentation rates for Site U1389. Mean Sedimentation rate
 498 is marked by dotted line.



499

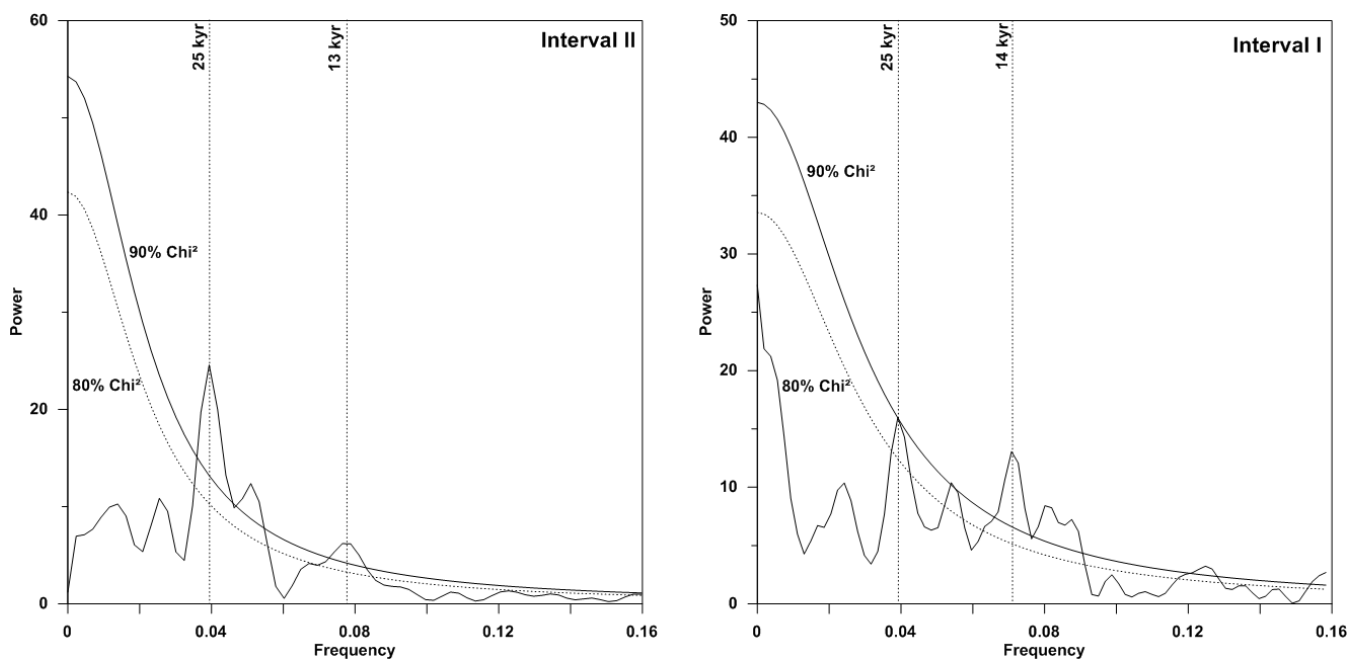


500

501 Figure 4: (A) UK37 based sea-surface temperature (SST) record of North Atlantic Site ODP 982 (Lawrence et al., 2009). The
 502 running mean has a band width of 23. AMOC phases are marked by black arrows and follow the chronology of Bell et al. (2015).
 503 (B) Benthic $\delta^{18}O$ records of both investigated intervals at Site U1389. Interval I comprises the time frame of 2.6 to 2.4 Ma and
 504 Interval II 2.1 to 1.8 Ma. Isotopic gradient between both records is indicated by the grey-shaded area. (C) Comparison of $\delta^{13}C$ of
 505 *P. ariminensis* for both investigated intervals at Site U1389 and $\delta^{13}C$ of the MedSea stack (Lourens et al. 1996, unpublished data).
 506 The running means have a band width of 5. The *C. ungerianus* based $\delta^{13}C$ values of the MedSea stack were adjusted to *P.*
 507 *ariminensis* $\delta^{13}C$ values of Site U1389 following the interspecies correction presented in Kaboth et al., (in prep) (D) Grain-size (63 -
 508 $150 \mu\text{m}$ wt.-%) records for both investigated intervals at Site U1389. The filtered ~ 23 kyr signal of the grain-size signal is indicated
 509 by the black dotted-line. Sapropel mid-points are marked by orange arrows and follow the chronology of Emeis et al. (2000).



510



511

512 **Figure 5: REDFIT Power Spectra of the grain-size values (63-150µm fraction in wt.-%) for both investigated intervals of Site**
513 **U1389 (Interval I = 2.6-2.4 Ma ; Interval II: 2.1-1.8 Ma). The 90% (red) and 80% (blue) confidence levels are given.**



514

No.	Event	TOP Depth (mbsf)	BOT Depth (mbsf)	Time (Ma)	Reference
1	Top Olduvai	542.00		1.806	1
2	Bottom Olduvai		592.00	1.945	1
3	Matuyama/Gauss	696.00		2.588	1
4	LO <i>C. macintyrie</i>	510.09	515.65	1.66	2
5	FO <i>G. inflata</i>	627.21	630.21	2.09	3
6	LO <i>G. puncticulata</i>	645.02	646.61	2.41	3
7	LO <i>D. pentradiatus</i>	674.25	681.98	2.5	2
8	LO <i>D. scurlus</i>	681.98	693.70	2.53	2
9	LO <i>D. tamalis</i>	~805		2.8-2.87	4

515

516 **Table 1: Paleomagnetic and biostratigraphic tie points used in the primary age model of Site U1389 based on shipboard data**
 517 **following Hernández-Molina et al. (2013) and Stow et al. (2013). 1 = Gradstein et al. (2012); 2 = Raffi et al. (2006); 3= Lourens et**
 518 **al. (2004); 4 = Grunert P., pers. comm.**



519

Depth (mbsf)	Age (ka)
512	1660
542	1806
551.25	1828
554	1851
564	1861
570	1867
574	1875
580	1898
592.00	1945
595.00	1965
600	1975
615.63	2005
623.00	2070
629.1	2092
629.75	2117.5
631.1	2132.5
646	2425
648.75	2435.5
665.1	2462.5
666.3	2486
673	2500
677.45	2517.5
687	2539
689	2552
691.5	2560
693.5	2583
696	2588
805	2800

520 **Table 2: Paleomagnetic and biostratigraphic tie points used in the primary age model of Site U1389 based on shipboard data**
521 **following Hernández-Molina et al. (2013) and Stow et al. (2013). 1 = Gradstein et al. (2012); 2 = Raffi et al. (2006); 3= Lourens et**
522 **al. (2004); 4 = Grunert P., pers. comm**